Progress towards quantum simulating the classical O(2) model

Haiyuan Zou,[1] Yuzhi Liu,[2] Chen-Yen Lai,[3] J. Unmuth-Yockey,[1] Li-Ping Yang,[4] A. Bazavov,[1,3] Z. Y. Xie,[5] T. Xiang,[5] S. Chandrasekharan,[6] S.-W. Tsai,[3] and Y. Meurice[1]

[1]*Department of Physics and Astronomy, The University of Iowa, Iowa City, Iowa 52242, USA*
[2]*Department of Physics, University of Colorado, Boulder, Colorado 80309, USA*
[3]*Department of Physics and Astronomy, University of California, Riverside, California 92521, USA*
[4]*Department of Physics, Chongqing University, Chongqing 400044, China*
[5]*Institute of Physics, Chinese Academy of Sciences, P.O. Box 603, Beijing 100190, China*
[6]*Department of Physics, Duke University, Durham, North Carolina 27708, USA*

(Received 26 March 2014; revised manuscript received 9 October 2014; published 1 December 2014)

We connect explicitly the classical O(2) model in $1+1$ dimensions, a model sharing important features with U(1) lattice gauge theory, to physical models potentially implementable on optical lattices and evolving at physical time. Using the tensor renormalization-group formulation, we take the time continuum limit and check that finite-dimensional projections used in recent proposals for quantum simulators provide controllable approximations of the original model. We propose two-species Bose-Hubbard models corresponding to these finite-dimensional projections at strong coupling and discuss their possible implementations on optical lattices using a ^{87}Rb and ^{41}K Bose-Bose mixture.

DOI: 10.1103/PhysRevA.90.063603 PACS number(s): 03.75.Lm, 03.67.Ac, 11.15.Ha, 37.10.Jk

I. INTRODUCTION

Recently, there has been a lot of interest in the possibility of building quantum simulators for lattice gauge theory (LGT) using optical lattices [1–5]. The goal is to engineer many-body systems with cold atoms that can be built experimentally and that approximately evolve according to some given quantum LGT Hamiltonian. Achieving this goal would allow us to go beyond what can be done with classical computing, namely overcoming the sign problem of quantum chromodynamics (QCD) with a chemical potential, establishing its phase diagram, and studying its real-time evolution. Introducing a chemical potential in QCD is necessary to describe physical situations in which a nonzero quark density is needed, such as the early universe or heavy-ion collisions. Building a quantum simulator for QCD requires that we first systematically establish the viability of the approach by building up on simple models sharing some of the basic features of lattice QCD.

In the context of condensed matter, a proof of principle that quantum simulating is possible has been given in the case of the Bose-Hubbard model. For this simple model, a remarkable level of *quantitative* agreement [6] has been reached between state-of-the-art quantum Monte Carlo calculations and their experimental optical lattice implementations. It would be very desirable to provide a similar proof of principle in the context of LGT.

In this article, we propose an optical lattice setup and accurate numerical methods to relate it to a simple model that shares some important features (discrete imaginary time, relativistic space-time symmetry, compact gauge variables, and a complex action) with interesting LGT models, namely the classical O(2) in $1+1$ dimensions with a chemical potential. This model is described in Sec. II. The goal of the article is to discuss the optical lattice implementation of one of the building blocks of the Hamiltonian formulation of gauge theory, namely the "quantum rotors" that are described in more detail below, rather than discussing more specific aspects such as the implementation of Gauss's law for LGT models involving these building blocks.

The connection between the classical O(2) in $1+1$ dimensions and physical systems on optical lattices requires three steps. First, we introduce computational methods based on the tensor renormalization-group (TRG) method [7–10] to take the time continuum limit (step 1, Sec. II) and to calculate the effects of finite-dimensional truncations necessary for a physical implementation (step 2, Sec. III). We then construct a two species Bose-Hubbard model which at second order in degenerate perturbation theory can be matched with the finite-dimensional truncations, and we propose an experimental implementation using a ^{87}Rb and ^{41}K Bose-Bose mixture (step 3, Sec. IV). The O(2) model is very well understood using classical computing [7–12], and our goal is not to learn more about this model from quantum simulations but rather to demonstrate that a quantitative correspondence is possible.

One should be aware of the fact that in contrast to the quantum Monte Carlo treatment of condensed-matter models where space and time are completely independent entities, the state-of-the-art calculations in LGT are performed using the Lagrangian formalism at discrete imaginary time where space and time are completely interchangeable. In LGT, the continuum limit is usually taken in a way that preserves this relativistic symmetry between space and time. The Hamiltonian representation provides the functional forms used to fit correlation functions, and a slightly better resolution in the time direction is sometimes used, however the time continuum limit is not taken independently. Explicit Hilbert space representations of the physical states and of their matrix elements are mostly absent from today's lattice QCD calculations. In our construction, the first step will be to take the time continuum limit using the Lagrangian formulation. Note that Lorentz symmetry can emerge near criticality in the Hamiltonian formulation [13] and that the classical O(2) model is often used as an effective theory for the Bose-Hubbard model [14].

It is important to understand the similarity between the infinite-dimensional Hilbert spaces of the O(2) model and U(1) LGT in the Hamiltonian formulation. In the mid-1970s, LGTs were developed in the Hamiltonian formalism [15–18]

using local gauge variables that live on bonds connecting neighboring sites. For continuous and compact symmetry groups, these gauge links are operators that live on an infinite Hilbert space and in the appropriate basis look like classical group elements. In U(1) LGT [16], gauge links are phases $e^{i\theta}$, which, when considered as operators, live in an infinite-dimensional Hilbert space spanned by the eigenstates $|n\rangle$ of the "angular momentum" operator $L = -i\partial/\partial\theta$ with all positive *and* negative integer eigenvalues n. The same "quantum rotors" appear in the Hamiltonian formulation of the O(2) model [17,18].

For realistic implementations with cold atoms, it is necessary to consider Hamiltonians where gauge links are quantum operators that live in a finite rather than infinite Hilbert space [19,20]. In the U(1) example, this would mean the eigenvalues of L only take a finite range of values. For this to occur naturally, one restricts the Hilbert space to be in a spin-s representation, i.e., $n = -s, -(s-1), \ldots 0, \ldots (s-1), s$. Finite-dimensional projections and quantum link variables have played an important role in recent proposals to simulate dynamical gauge fields [1–3,21,22].

The common features of the O(2) model considered here and the U(1) gauge model can be understood by comparing the TRG formulations of the two models [8]. In both cases, the Fourier expansion of $\exp[\beta\cos(\theta)]$ is used, which leads to the labeling of states by (positive and negative) integers. However, the quantum numbers are associated with plaquettes in the gauge case rather than links in the spin case. The physics of the models is also quite different. For instance, in $2+1$ dimensions, the O(2) spin model has a second-order phase transition while the U(1) gauge model has none.

II. THE MODEL AND ITS TIME CONTINUUM LIMIT

The simplest model involving the quantum rotors described above is the O(2) model in $1+1$ dimensions. Its partition function reads

$$Z = \int \prod_{(x,t)} \frac{d\theta_{(x,t)}}{2\pi} e^{-S}, \tag{1}$$

with action

$$S = -\beta_\tau \sum_{(x,t)} \cos(\theta_{(x,t+1)} - \theta_{(x,t)} - i\mu) - \beta_s \sum_{(x,t)} \cos(\theta_{(x+1,t)} - \theta_{(x,t)}). \tag{2}$$

The meaning of the chemical potential μ [23] appears clearly in the limit where β_s is zero and we have decoupled quantum rotors with a discrete spectrum labeled by n_x at each site x [see Eq. (5)]. Using these labels, the chemical potential generates a contribution $-\mu n_x$ to the energy at each site. The sites of the rectangular $N_s \times N_\tau$ lattice are labeled as (x,t) and we assume periodic boundary conditions in space and time.

When $\beta_\tau \gg \beta_s$, we obtain the time continuum limit [17,18,24] with a Hamiltonian connecting quantum rotors on a lattice with β_s acting as the coupling between the spatial sites. In the $\otimes_x |n_x\rangle$ basis, it reads

$$\hat{H} = \frac{\tilde{U}}{2} \sum_x \hat{L}_x^2 - \tilde{\mu} \sum_x \hat{L}_x - \tilde{J} \sum_{\langle xy \rangle} \cos(\hat{\theta}_x - \hat{\theta}_y), \tag{3}$$

with $\tilde{U} = 1/(\beta_\tau a)$, $\tilde{\mu} = \mu/a$, and $\tilde{J} = \beta_s/a$, the sum extending over sites x and nearest neighbors $\langle xy \rangle$ of the space lattice, and a is a lattice spacing.

The commutation relations $[L, e^{\pm i\hat{\theta}}] = \pm e^{\pm i\hat{\theta}}$ show that $e^{\pm i\hat{\theta}}$ act like creation and annihilation operators. However, there is no eigenstate of L annihilated by $e^{-i\hat{\theta}}$. At large μ, there is an effective truncation [25,26] that makes the eigenstates with negative eigenvalues irrelevant. For small values of μ, we will consider the quantum link inspired truncation where the original operator algebra is approximated by a spin-s representation with $|n| \leqslant s$.

Remembering the role played by the differential operator $L = -i\partial/\partial\theta$ in the construction of the spherical harmonics, we replace L by L^3, the third component of the angular momentum in the SU(2) Lie algebra. Pursuing the analogy, we replace $e^{\pm i\hat{\theta}}$ by an operator proportional to the raising and lowering operators $L^\pm$ in the spin-s representation. In the case of spin-1, a comparison of the matrix elements shows that the correspondence between the two representations can be accomplished by properly choosing the constant of proportionality.

III. NUMERICAL CALCULATION OF THE PHASE DIAGRAM

We now discuss the phase diagram, the finite spin projection, and the time continuum limit by using the TRG method. Following the procedure described in Refs. [8–10], we can write

$$Z = \mathrm{Tr} \prod_{(x,t)} T^{(x,t)}_{n_x n'_x n_t n'_t}, \tag{4}$$

with the local tensor expressed in terms of the modified Bessel functions:

$$T^{(x,t)}_{n_x n_{x'} n_t n_{t'}} = \sqrt{I_{n_t}(\beta_\tau) I_{n_{t'}}(\beta_\tau) \exp[\mu(n_t + n'_t)]} \times \sqrt{I_{n_x}(\beta_s) I_{n_{x'}}(\beta_s)} \delta_{n_x + n_t, n_{x'} + n_{t'}}. \tag{5}$$

The indices n_x, n'_x, n_t, and n'_t label the four links coming out of (x,t) in the x and t direction, and the trace Tr refers to the sum over all these link indices. A transfer matrix $\mathbb{T}$ can be constructed by taking the spatial traces in a time slice:

$$\mathbb{T}_{(n_1, n_2, \ldots, n_{N_s})(n'_1, n'_2, \ldots, n'_{N_s})} = \sum_{n_{x1} n_{x2} \ldots n_{N_s}} T^{(1,t)}_{n_{xN_s} n_{x1} n_1 n'_1} T^{(2,t)}_{n_{x1} n_{x2} n_2 n'_2, \ldots} \cdots T^{(N_s,t)}_{n_{x(N_s-1)} n_{xN_s} n_{N_s} n'_{N_s}}. \tag{6}$$

The indices $(n_1, n_2, \ldots, n_{N_s})$ represent the past and $(n'_1, n'_2, \ldots, n'_{N_s})$ the future.

In view of the rapid decay of the $I_n(\beta)$ when $|n|$ increases at fixed β, good approximations can be obtained by replacing the infinite sums by sums restricted to $-n_{\max}$ to $n_{\max}$. We denote the number of states $D_{st} = 2n_{\max} + 1$. With this truncation, the transfer matrix is a $D_{st}^{N_s} \times D_{st}^{N_s}$ matrix. It is possible to

TABLE I. $\langle N\rangle$ for the worm algorithm and the HOTRG for $\beta_s = \beta_\tau = \beta$.

β	μ	$\langle N\rangle$ (worm)	$\langle N\rangle$ (HOTRG)
1.12	0.01	0.00726(1)	0.00728(8)
0.46	1.8	0.98929(1)	0.9892(3)
0.28	2.85	1.98980(2)	1.989(2)
0.2	3.53	2.96646(3)	2.967(1)
0.12	4.3	3.96206(4)	3.965(1)

coarse grain the transfer matrix efficiently by using a higher-order singular value decomposition (HOTRG) described in Ref. [7]. This procedure then reduces the two-site transfer matrix to a $D_{st} \times D_{st}$ matrix and thus accomplishes the blocking from two sites to a single site. Note that in the spin-1 projection we keep D_{st} much larger than 3 as we keep blocking. In other words, the spin projection represents a microscopic modification of the model, while we need to keep D_{st} as large as possible in order to maintain good macroscopic accuracy. The same numerical method is used in all cases, the only difference being the initial tensor.

An important advantage of the TRG method is that it allows us to reach exponentially large volumes. However, it is important to check the results at small volume where sampling methods are feasible and accurate. We have used the TRG and the worm algorithm [11,12] to calculate the particle number density [12]

$$\langle N\rangle \equiv 1/(N_s \times N_\tau)\partial \ln Z/\partial\mu. \tag{7}$$

The partition function Z can be calculated by taking the trace of $\mathbb{T}^{N_\tau}$ or by using the methods described in Refs. [7–10]. The numerical values on a 16×16 lattice, for values of $\beta_s = \beta_\tau$ and μ slightly below the tips of the regions with $\langle N\rangle = 0,1,\ldots,4$ of the phase diagram described below, are shown in Table I.

Small discrepancies between the two methods appear typically in the fourth significant digit. The errors for the worm algorithm are purely statistical, and to the best of our knowledge, there are no systematic errors associated with it. On the other hand, for the TRG method, the limit $D_{st} \to \infty$ shows very small variations, which will be documented and analyzed in a separate publication [27] but do not affect the results presented here.

By increasing μ at fixed β, we go through successive Mott insulating (MI) phases characterized by a fixed integer value of $\langle N\rangle$ increasing with μ and alternating with superfluid (SF) phases where $\langle N\rangle$ interpolates continuously between the successive integers. The phase boundaries are clearly visible from the steps in $\langle N\rangle$ as a function of μ, as shown in Fig. 1. The phase boundaries can also be obtained by looking at the two largest eigenvalues of the transfer matrix. In a given MI phase, one would expect that the largest value of the transfer matrix is unique and corresponds to an eigenstate with fixed integer particle density. On the other hand, in the SF phase, the two largest eigenvalues of the transfer matrix are expected to be degenerate and the corresponding eigenstates are expected to have particle density corresponding to the two neighboring MI regions. Figure 1 shows that these expectations are verified

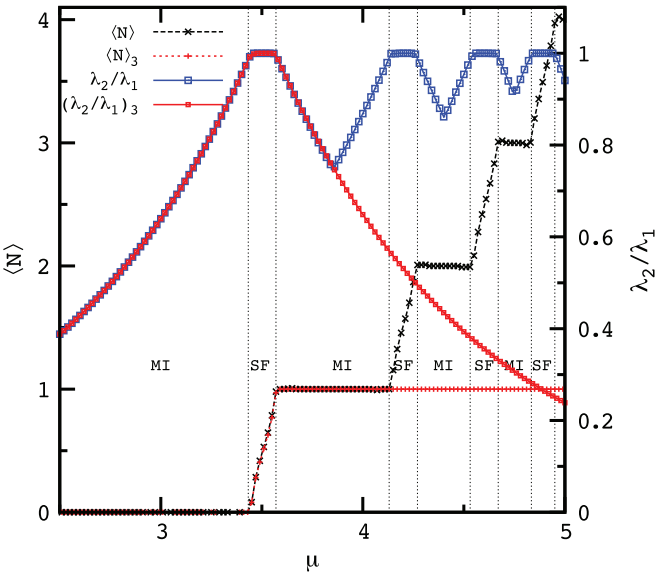

FIG. 1. (Color online) The ratio (λ_2/λ_1) of the first two eigenvalues of the transfer matrix and the particle number density $\langle N\rangle$ for the $\beta_\tau = \beta_s = 0.06$ from the HOTRG calculation with $D_{st} = 15$. The particle number density $\langle N\rangle_3$ and the second normalized eigenvalues $(\lambda_2/\lambda_1)_3$, where a lower index 3 denotes the spin-1 projection (three-state), are also shown.

quite precisely. The system reaches the superfluid (SF) phase when $\lambda_2/\lambda_1 = 1$, and when μ is increased further, this ratio remains 1 while there is an increase in the particle number density between two adjacent integers, which stand for two different MI phases.

The alternation between the MI and SF phases in the β-μ plane is shown in Fig. 2. The pointy shape of the MI phase region is also observed in other $(1+1)$-dimensional Bose-Hubbard models [28,29]. The spin-1 projection is also shown in these figures. When μ is not too large, only small

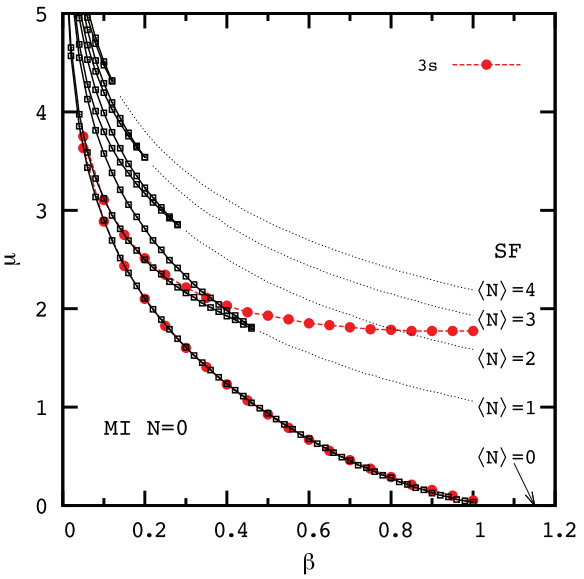

FIG. 2. (Color online) The phase diagram in the β-μ plane for the isotropic ($\beta_s = \beta_\tau = \beta$) case.

differences with the original, unprojected model are observed. However, when μ becomes large enough to have $\langle N\rangle > 1$, the truncation prevents such a large occupation and $\langle N\rangle$ saturates to 1 as expected, and there is no $\langle N\rangle = 2$ MI phase. The phase boundary in Fig. 2 between the MI $\langle N\rangle = 0$ phase from the SF phase coincides approximately with the line for the model with an infinite number of states. Similarly, the spin-2 projection (not shown on the graph) reproduces well the $\langle N\rangle = 0$ and 1 boundaries while discrepancies appear for $\langle N\rangle = 2$.

Figure 2 shows that when β is small, the boundary between the MI and SF phase appears to be at large values of μ. It is useful to recall that so far we have only considered the phase diagram in the isotropic case $\beta = \beta_s = \beta_\tau$. When $\beta \to 0$, the interaction along the space links is small, but if μ is sufficiently large, the interactions along the time links are not small. In the limit where the interactions among the space links are negligible, the problem reduces to a collection of independent one-site problems (simple quantum mechanics) as in mean-field theory [14]. In this limit, Eq. (5) shows that the transfer matrix becomes diagonal because $I_n(0) = 0$ except for $n = 0$ [$I_0(0) = 1$], and by the conservation law the same index n_x characterizes the interaction along the time direction. In other words, there is no quantum number flowing in the space direction, and the flow in the time direction at each site is constant. In this limit, the eigenvalues of the transfer matrix are just

$$\lambda_{(n_1,n_2,\ldots,n_{N_s})} = \prod_x I_{n_x}(\beta) e^{n_x \mu}. \tag{8}$$

The largest eigenvalue is then

$$\lambda_{\max} = \{\max_n [I_n(\beta) e^{n\mu}]\}^{N_s}. \tag{9}$$

Finding the value of n corresponding to the maximum eigenvalue gives the particle density $\langle N\rangle$ in the MI phase.

The maximization of $A_n = I_n(\beta) e^{n\mu}$ can be achieved by considering the ratios $r_n = A_{n+1}/A_n$. Note that we assume $\mu > 0$, and given that $I_n(\beta) = I_{-n}(\beta)$, we only need to consider $n \geqslant 0$. When $r_{n-1} > 1$ and $r_n < 1$, A_n is a maximum. It can be shown in the limit of small and large β that r_n decreases when n increases. If this remains true for arbitrary β and if $r_n \neq 1$, then the problem has a unique solution. The interesting case is $r_n = 1$, which implies $A_n = A_{n+1}$ and should be at the boundary between two MI phases with particle density n and $n+1$. In the small-β limit, $I_n(\beta) \simeq \beta^n/(2^n n!)$ and the condition $r_n = 1$ implies that

$$\beta e^{\mu}/2 = n + 1 \tag{10}$$

in that approximation. The sudden transition in particle density occurs at integer values of $\beta e^{\mu}/2$. This prediction is confirmed by plotting the phase diagram in the β-$\beta e^{\mu}/2$ plane as shown in Fig. 3. We see that by changing the vertical coordinate to $\mu \to \beta e^{\mu}/2$, the shape of the phase diagram of the isotropic system looks like the cuspy shapes found for the Bose-Hubbard model in one spatial dimension [28,29]. Keeping in mind that we are working in the limit of small β, Eq. (10) implies that the phase boundaries of the SF phase between the n and $n+1$ MI phases diverge like $\ln[2(n+1)/\beta]$ when $\beta \to 0$, which is consistent with Fig. 2.

We now depart from the isotropic $\beta_\tau = \beta_s$ situation and consider the case $\beta_\tau \gg \beta_s$ corresponding to the time continuum limit. If we neglect β_s, we obtain the one-site approximation described above. The particle density can be obtained from the ratio analysis in the large-β_τ limit. Using $I_{n+1}(\beta_\tau)/I_n(\beta_\tau) \simeq 1 - (n+1/2)/\beta_\tau$ in this limit, we find that the degeneracy occurs for integer values of $\mu\beta_\tau - 1/2$. Defining the effective chemical potential $\mu_e = \mu\beta_\tau - 1/2$ and effective coupling $\beta_e = \beta_s\beta_\tau$, we find that the same MI-SF pattern appears in the β_e-μ_e plane (Fig. 4).

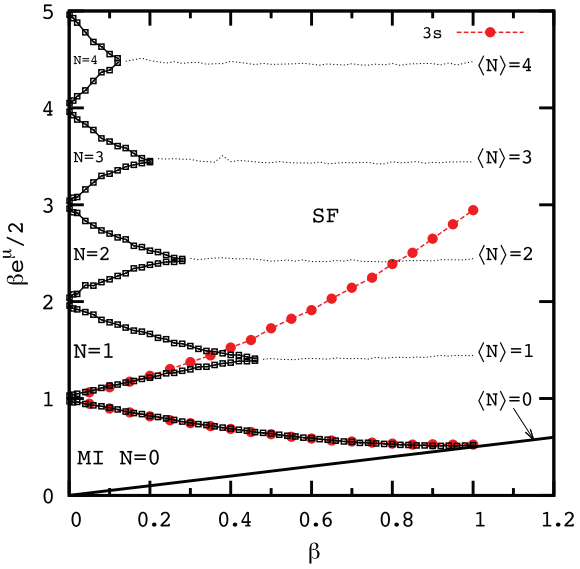

FIG. 3. (Color online) The phase diagram in the β-$\beta e^{\mu}/2$ plane for the isotropic case. $\langle N\rangle = 0$ ($\mu = 0$) line in the SF phase is the Kosterlitz-Thouless phase in the $1+1$D O(2) model at $\mu = 0$. The lines labeled by "3s" stand for the phase boundaries of the spin-1 (three-state) system.

Having computed the phase diagram in the $\beta_\tau = \beta_s$ and $\beta_\tau \gg \beta_s$ cases, we learned that they have very similar shapes in suitable systems of coordinates. From this we expect that

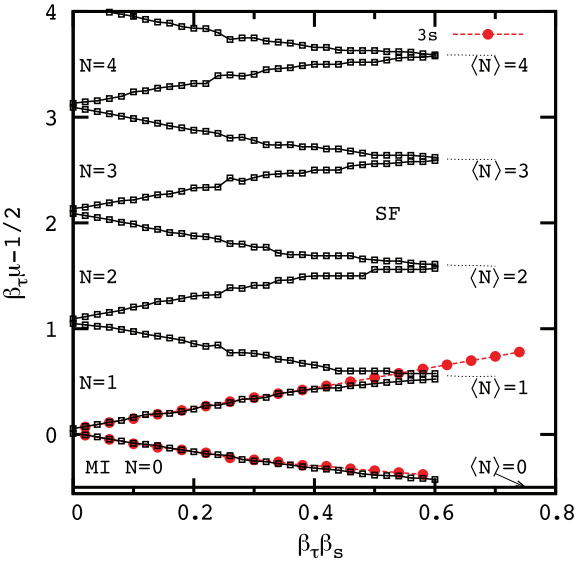

FIG. 4. (Color online) The phase diagram for the $1+1$D O(2) model at $\beta_\tau = 10$ in the β_e-μ_e plane is shown. The lines labeled by "3s" stand for the phase boundaries of the spin-1 (three-state) system.

they can be smoothly deformed into each other and that nothing special happens in the intermediate situations.

IV. OPTICAL LATTICE IMPLEMENTATION

To incorporate the positive and negative eigenvalues of L, we will consider a two-species Bose-Hubbard Hamiltonian on a lattice:

$$\mathcal{H} = -\sum_{\langle xy\rangle}(t_a a_x^\dagger a_y + t_b b_x^\dagger b_y + \text{H.c.}) - \sum_{x,\alpha}(\mu + \Delta_\alpha) n_x^\alpha + \sum_{x,\alpha}\frac{U_\alpha}{2} n_x^\alpha\left(n_x^\alpha - 1\right) + W\sum_x n_x^a n_x^b + \sum_{\langle xy\rangle,\alpha} V_\alpha n_x^\alpha n_y^\alpha \tag{11}$$

with $\alpha = a,b$ indicating the two different species, $n_x^a = a_x^\dagger a_x$ and $n_x^b = b_x^\dagger b_x$ the number operators, and $|n_x^a, n_x^b\rangle$ the corresponding on-site basis. This class of models has been studied extensively [30–33]. It is possible to adjust the chemical potentials in order to set $\langle n_x\rangle = \langle n_x^a + n_x^b\rangle = 2$. In the limit where $U_a = U_b = W$ are very large and positive, the on-site Hilbert space can then be restricted to the states satisfying $n_x = 2$ at each site. All the other states (with $n_x \neq 2$) belong to high-energy sectors that are separated from this one by energies of order U. The three states $|2,0\rangle$, $|1,1\rangle$, and $|0,2\rangle$ correspond to the three states of the spin-1 projection considered above.

It is useful to visualize the minima of the on-site Hamiltonian obtained in the limit $t \to 0$. It can be written as a quadratic form and a linear term in n_a and n_b. If $U_a U_b > W^2$, there is a unique minimum, $|1,1\rangle$, which corresponds to a miscible phase where the two species need to be present at the same place. Since in the spin-1 approximation, $|1,1\rangle$ corresponds to a rotor with angular momentum zero, this is the correct situation for the O(2) model we try to simulate. On the other hand, if $U_a U_b < W^2$, the extremum is a saddle point. As we will discuss later, the unstable direction coming out of the extremum is limited by the positivity of the occupation number. There are two vacua $|2,0\rangle$ and $|0,2\rangle$, which corresponds to immiscible phases. The limiting case $U_a U_b = W$ corresponds to our $U_a = U_b = W = U_0$ lowest-order approximation. If in addition we have $\mu = (3/2)U_0$ and $\Delta_\alpha = 0$, we have a flat direction along the line $n_x = 2$ where we have three states of energy $-2U_0$, while the degenerate lines with $n_x = 1$ or 3 have energy $-(3/2)U_0$, which is considered much larger in the strong-coupling approximation. Small changes in the parameters will break the degeneracy of the ground state but preserve a significant difference between these states and the excited states. Decreasing W lowers the energy of the $|1,1\rangle$ state linearly in the difference with U_0. Similarly, increasing W raises the energy of the $|1,1\rangle$, the flat direction curves down at both ends, but the positivity of the occupation number prevents the energy from being unbounded from below. When species-dependent chemical potentials are turned on, the flat direction becomes slanted linearly in the variation of the chemical potential Δ_α. The overall shape of the trap will typically create small variations in a space-dependent manner. In summary, as long as the variations of the parameters are small compared to U_0, the features departing from the degenerate case can be treated as perturbations.

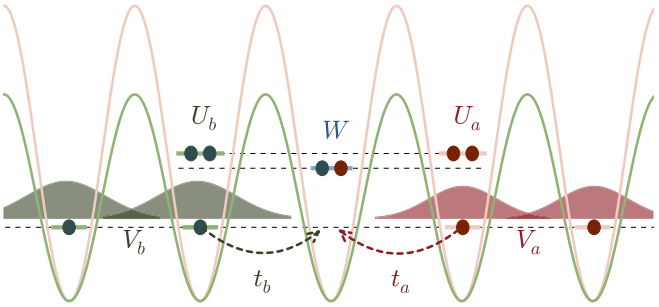

FIG. 5. (Color online) Two species (green and red) of bosons on species-dependent optical lattices (with the same color). The nearest-neighbor interaction is coming from the overlap of Wannier Gaussian wave functions. We assume the difference between intraspecies interactions are small $U \gg \delta$.

Going back to the general Hamiltonian [Eq. (11)], we write $U_{a(b)} = U \pm \delta$ and assume $U \gg \delta, (U - W), V, t_\alpha, \Delta_\alpha$ and do degenerate perturbation theory. Virtual processes exchanging particles between neighboring sites are allowed at second order with contributions proportional to $-t_\alpha t_{\alpha'}/U$. The hopping amplitude is tunable, and when chosen to be $t_\alpha = \sqrt{V_\alpha U/2}$, the final result is that the effective Hamiltonian up to second order in degenerate perturbation theory corresponds to the spin-1 projection of the rotor Hamiltonian of Eq. (3) with $\tilde{J} = \sqrt{V_a V_b}$, $\tilde{U} = 2(U - W)$, and $\tilde{\mu} = (\Delta_a - V_a) - (\Delta_b - V_b)$. Similarly, by increasing the chemical potentials, it is possible to restrict the Hilbert space to $n_x^a + n_x^b = 2s$, which corresponds to a spin-s projection in the O(2) model.

This two-species Bose-Hubbard model can be realized in a ^{87}Rb and ^{41}K Bose-Bose mixture where an interspecies Feshbach resonance is accessible [34,35]. Due to the physical nature of the different atoms, the hopping amplitudes (t_a, t_b) are different to begin with, as well as the intraspecies interactions. In addition, species-dependent optical lattices [36–40] are widely used in boson systems, which allows the hopping amplitudes of each individual species to be further tuned to the desired value. As mentioned above, the interspecies interaction (W) can be controlled by an external magnetic field [35]. Finally, the extended repulsion, V_α, is present and small when we consider Wannier Gaussian wave functions centered on nearby lattice sites according to previous study [41]. This is schematically illustrated in Fig. 5. This may be the most difficult parameter to achieve, but other proposals may be explored, such as by using dipolar bosons [42], or by pumping bosons to higher Bloch bands [43] in order to engineer the nearest-neighbor interaction. It is also important to have U significantly larger than the temperature. For the mixture considered here, the temperature and recoil energies are of the order of 100 nK, and values of U 10–20 times larger can typically be reached [35,44,45].

V. CONCLUSIONS

In summary, we have used recently developed numerical methods to connect the O(2) model in $1+1$ dimensions to an optical lattice setup. A first test of the correspondence would be to check that the optical lattice system reproduces

the phase diagram of Fig. 4, which corresponds to the time continuum limit $\beta_\tau \gg \beta_s$ of the classical model and where the microscopic parameters can be approximately connected to those of the two-species Hubbard model.

The TRG method presented here allows reliable calculations of the eigenvalues λ_i of the transfer matrix. In the time continuum limit, we have

$$\lambda_i/\lambda_1 \propto e^{-a(E_i-E_0)}, \tag{12}$$

with E_i the corresponding energies and $a \propto 1/\beta_\tau$ the lattice spacing. Recently developed experimental techniques, e.g., momentum-resolved Bragg spectroscopy [46], could in principle allow detailed comparisons.

We have shown that for low enough μ, the effect of the truncation to spin-1 or -2 of the original O(2) model had small effects on the phase boundaries. In the TRG formulation, this truncation only affects the initial values of the tensor, which can be compared with the initial tensor of other spin models with a finite number of states in configuration space (clock and Potts models). Understanding how the symmetries of this initial tensor affect the universality class is under study.

The O(2) model has an exact conservation law that is made clear by the Kronecker δ in Eq. (5). The states kept in the TRG calculation have a well-defined quantum number associated with this conservation law, and it can monitored and put into histograms [27]. This provides detailed information about the average occupation and its fluctuations. It could give better insight into the validity of the Gutzwiller ansatz or mean-field calculations such as the ones discussed in Ref. [14], or the validity of the finite spin projection discussed here.

In LGT calculations, important information regarding the spectrum and matrix elements can be extracted from the two- and three-point functions obtained by introducing localized sources in the Lagrangian formulations. Techniques to gather related information from an optical lattice system have yet to be developed. Generalizing the work done here for the O(3) model, which has physics more similar to lattice QCD, seems possible and interesting.

ACKNOWLEDGMENTS

We thank Masanori Hanada, Peter Orland, Lode Pollet, Boris Svistunov, the participants of the Math-Physics and Particle and Nuclear Seminar at the University of Iowa, and of SIGN 2014 for stimulating discussions. This research was supported in part by the Department of Energy under DOE Grants No. DE-FG02-05ER41368, No. DE-SC0010114, and No. DE-FG02-91ER40664, by the Army Research Office of the Department of Defense under Award No. W911NF-13-1-0119, and NSF under Grant No. DMR-1411345. Part of the simulations were done at CU Boulder Janus clusters, and Y. L. thanks D. Mohler and J. Simone for discussions on code development.

[1] D. Banerjee, M. Bögli, M. Dalmonte, E. Rico, P. Stebler, U.-J. Wiese, and P. Zoller, Phys. Rev. Lett. **110**, 125303 (2013).
[2] E. Zohar, J. I. Cirac, and B. Reznik, Phys. Rev. Lett. **110**, 125304 (2013).
[3] L. Tagliacozzo, A. Celi, A. Zamora, and M. Lewenstein, Ann. Phys. (NY) **330**, 160 (2013).
[4] Y. Liu, Y. Meurice, and S.-W. Tsai, PoS (**Lattice 2012**), 246 (2012).
[5] U.-J. Wiese, Ann. Phys. **525**, 777 (2013).
[6] S. Trotzky, L. Pollet, F. Gerbier, U. Schnorrberger, I. Bloch, N. V. Prokofev, B. Svistunov, and M. Troyer, Nat. Phys. **6**, 998 (2010).
[7] Z. Y. Xie, J. Chen, M. P. Qin, J. W. Zhu, L. P. Yang, and T. Xiang, Phys. Rev. B **86**, 045139 (2012).
[8] Y. Liu, Y. Meurice, M. P. Qin, J. Unmuth-Yockey, T. Xiang, Z. Y. Xie, J. F. Yu, and H. Zou, Phys. Rev. D **88**, 056005 (2013).
[9] J. F. Yu, Z. Y. Xie, Y. Meurice, Y. Liu, A. Denbleyker, H. Zou, M. P. Qin, J. Chen, and T. Xiang, Phys. Rev. E **89**, 013308 (2014).
[10] A. Denbleyker, Y. Liu, Y. Meurice, M. P. Qin, T. Xiang, Z. Y. Xie, J. F. Yu, and H. Zou, Phys. Rev. D **89**, 016008 (2014).
[11] N. Prokof'ev and B. Svistunov, Phys. Rev. Lett. **87**, 160601 (2001).
[12] D. Banerjee and S. Chandrasekharan, Phys. Rev. D **81**, 125007 (2010).
[13] B. Capogrosso-Sansone, N. V. Prokof'ev, and B. V. Svistunov, Phys. Rev. B **75**, 134302 (2007).
[14] M. P. A. Fisher, P. B. Weichman, G. Grinstein, and D. S. Fisher, Phys. Rev. B **40**, 546 (1989).
[15] J. Kogut and L. Susskind, Phys. Rev. D **11**, 395 (1975).
[16] T. Banks, L. Susskind, and J. Kogut, Phys. Rev. D **13**, 1043 (1976).
[17] E. Fradkin and L. Susskind, Phys. Rev. D **17**, 2637 (1978).
[18] J. B. Kogut, Rev. Mod. Phys. **51**, 659 (1979).
[19] P. Orland and D. Rohrlich, Nucl. Phys. B **338**, 647 (1990).
[20] S. Chandrasekharan and U. Wiese, Nucl. Phys. B **492**, 455 (1997).
[21] E. Zohar, J. I. Cirac, and B. Reznik, Phys. Rev. Lett. **109**, 125302 (2012).
[22] D. Banerjee, M. Dalmonte, M. Müller, E. Rico, P. Stebler, U.-J. Wiese, and P. Zoller, Phys. Rev. Lett. **109**, 175302 (2012).
[23] P. Hasenfratz and F. Karsch, Phys. Lett. B **125**, 308 (1983).
[24] A. M. Polyakov, *Gauge Fields and Strings* (Harwood, Chur, Switzerland, 1987).
[25] M. P. A. Fisher, *Duality in Low Dimensional Quantum Field Theories, in Strong Interaction in Low Dimensions* (Kluwer Academic, Dordrecht, 2004).
[26] S. Sachdev, *Quantum Phase Transitions*, 2nd ed. (Cambridge University Press, Cambridge, 2011).
[27] L. P. Yang, H. Zou, Y. Liu, S. Chandrasekharan, J. Unmuth-Yockey, Z. Y. Xie, T. Xiang, and Y. Meurice (unpublished).
[28] G. G. Batrouni and R. T. Scalettar, Phys. Rev. B **46**, 9051 (1992).
[29] T. D. Kühner and H. Monien, Phys. Rev. B **58**, R14741 (1998).
[30] A. B. Kuklov and B. V. Svistunov, Phys. Rev. Lett. **90**, 100401 (2003).
[31] A. Kuklov, N. Prokofev, and B. Svistunov, Phys. Rev. Lett. **92**, 050402 (2004).
[32] P. Chen and M.-F. Yang, Phys. Rev. B **82**, 180510 (2010).

[33] C.-M. Chung, S. Fang, and P. Chen, Phys. Rev. B **85**, 214513 (2012).
[34] J. Catani, L. De Sarlo, G. Barontini, F. Minardi, and M. Inguscio, Phys. Rev. A **77**, 011603 (2008).
[35] G. Thalhammer, G. Barontini, L. De Sarlo, J. Catani, F. Minardi, and M. Inguscio, Phys. Rev. Lett. **100**, 210402 (2008).
[36] P. J. Lee, M. Anderlini, B. L. Brown, J. Sebby-Strabley, W. D. Phillips, and J. V. Porto, Phys. Rev. Lett. **99**, 020402 (2007).
[37] M. Anderlini, P. J. Lee, B. L. Brown, J. Sebby-Strabley, W. D. Phillips, and J. Porto, Nature (London) **448**, 452 (2007).
[38] D. McKay and B. DeMarco, New J. Phys. **12**, 055013 (2010).
[39] P. Soltan-Panahi, J. Struck, P. Hauke, A. Bick, W. Plenkers, G. Meineke, C. Becker, P. Windpassinger, M. Lewenstein, and K. Sengstock, Nat. Phys. **7**, 434 (2011).
[40] N. Belmechri, L. Förster, W. Alt, A. Widera, D. Meschede, and A. Alberti, J. Phys. B **46**, 104006 (2013).
[41] G. Mazzarella, S. M. Giampaolo, and F. Illuminati, Phys. Rev. A **73**, 013625 (2006).
[42] C. Trefzger, C. Menotti, and M. Lewenstein, Phys. Rev. Lett. **103**, 035304 (2009).
[43] V. W. Scarola and S. Sarma, Phys. Rev. Lett. **95**, 033003 (2005).
[44] J. Catani, G. Lamporesi, D. Naik, M. Gring, M. Inguscio, F. Minardi, A. Kantian, and T. Giamarchi, Phys. Rev. A **85**, 023623 (2012).
[45] I. Bloch, J. Dalibard, and W. Zwerger, Rev. Mod. Phys. **80**, 885 (2008).
[46] P. T. Ernst, S. Gotze, J. S. Krauser, K. Pyka, D.-S. Luhmann, D. Pfannkuche, and K. Sengstock, Nat. Phys. **6**, 56 (2010).